780 *Biochemistry* **2011,** *50,* 780–787
DOI: 10.1021/bi101733y

BIOCHEMISTRY
including biophysical chemistry & molecular biology
Article

Molecular Architecture of TylM1 from *Streptomyces fradiae*: An *N*,*N*-Dimethyltransferase Involved in the Production of dTDP-D-mycaminose[†,‡]

Amanda E. Carney and Hazel M. Holden*

Department of Biochemistry, University of Wisconsin, Madison, Wisconsin 53706, United States

Received October 28, 2010; Revised Manuscript Received November 30, 2010

ABSTRACT: D-Mycaminose is an unusual dideoxy sugar found attached to the antibiotic tylosin, a commonly used veterinarian therapeutic. It is synthesized by the Gram-positive bacterium *Streptomyces fradiae* as a dTDP-linked sugar. The last step in its biosynthesis involves the dimethylation of the hexose C-3′ amino group by an *S*-adenosylmethionine (SAM) dependent enzyme referred to as TylM1. Here we report two high-resolution X-ray structures of TylM1, one in which the enzyme contains bound SAM and dTDP-phenol and the second in which the protein is complexed with *S*-adenosylhomocysteine (SAH) and dTDP-3-amino-3,6-dideoxyglucose, its natural substrate. Combined, these two structures, solved to 1.35 and 1.79 Å resolution, respectively, show the orientations of SAM and the dTDP-linked sugar substrate within the active site region. Specifically, the C-3′ amino group of the hexose is in the correct position for an in-line attack at the reactive methyl group of SAM. Both Tyr 14 and Arg 241 serve to anchor the dTDP-linked sugar to the protein. To test the role of His 123 in catalysis, two site-directed mutant proteins were constructed, H123A and H123N. Both mutant proteins retained catalytic activity, albeit with reduced rates. Specifically, the k_{cat}/K_m was reduced to 1.8% and 0.37% for the H123A and H123N mutant proteins, respectively. High-resolution X-ray models showed that the observed perturbations in the kinetic constants were not due to major changes in their three-dimensional folds. Most likely the proton on the C-3′ amino group is transferred to one of the water molecules lining the active site pocket as catalysis proceeds.

Deoxyamino sugars represent an important and intriguing class of carbohydrates produced by various bacteria, fungi, and plants (*1*). These unusual sugars have been isolated, for example, from the *O*-antigens of Gram-negative bacteria or found attached to the aglycone rings of macrolide antibiotics. One such deoxyamino sugar, found on such antibiotics as midecamycin and tylosin, is D-mycaminose (*2*). As highlighted in Scheme 1, five enzymes are required for its production in *Streptomyces fradiae* (*3*−*5*). The first step, catalyzed by a nucleotidyltransferase referred to as TylA1, involves the attachment of α-D-glucose 1-phosphate to dTMP.[1] The nucleotidyl moiety serves as a recognition element for the subsequent enzymes in the pathway, and it also provides an excellent leaving group for the transfer of the modified sugar to the macrolide ring. In the next step shown in Scheme 1, the C-6′ hydroxyl group of the hexose is removed, and the C-4′ hydroxyl group is oxidized to a keto functionality yielding dTDP-4-keto-6-deoxyglucose. TylA2, an NAD-dependent 4,6-dehydratase, catalyzes this reaction. The first two steps in D-mycaminose biosynthesis are common to many of the pathways leading to the formation of unusual di- and trideoxy sugars, and both the nucleotidylyltransferases and the dehydratases have been well characterized with respect to structure and function (*6*, *7*). The third step in the biosynthesis of D-mycaminose involves a 3,4-ketoisomerization that is catalyzed by Ty1a. In the penultimate step, a PLP-dependent amination of the sugar C-3′ carbon occurs via the action of TylB.

The focus of this investigation, TylM1, is an *S*-adenosylmethionine- or SAM-dependent enzyme that catalyzes the last step in D-mycaminose biosynthesis, the dimethylation of the C-3′ amino group. Whereas methylation is a common theme in biology, most methyltransferases catalyze single methylations at carbons, oxygens, sulfurs, or nitrogens (*8*). Little is known, however, regarding enzymes that are capable of catalyzing *N*,*N*-dimethylations. Recently, the crystal structure of DesVI from *Streptomyces venezuelae* was reported from this laboratory (*9*). Like TylM1, it functions as an *N*,*N*-dimethyltransferase, but it is involved in the production of D-desoamine rather than D-mycaminose (*10*). Importantly, DesVI and TylM1 share an amino acid sequence identity of 60%, are homodimeric proteins, and display highly similar biochemical properties (*11*). While the structure of DesVI provided key information regarding the overall fold of the enzyme, details concerning its active site architecture were somewhat limited due to the lack of a bound nucleotide-linked sugar substrate. Here we report a combined structural and functional investigation of TylM1 from *S. fradiae*. For this analysis, two high-resolution structures were determined: one complexed with SAM and dTDP-phenol and the other with bound *S*-adenosylhomocysteine (SAH) and its natural

[†]This research was supported in part by an NIH grant (DK47814 to H.M.H.).

[‡]X-ray coordinates have been deposited in the Research Collaboratory for Structural Bioinformatics, Rutgers University, New Brunswick, NJ (accession numbers 3PFG, 3PFH, 3PX2, and 3PX3).

*To whom correspondence should be addressed. E-mail: Hazel_Holden@biochem.wisc.edu. Fax: 608-262-1319. Phone: 608-262-4988.

[1]Abbreviations: HEPPS, 3-[4-(2-hydroxyethyl)-1-piperazinyl]propanesulfonic acid; IPTG, isopropyl β-D-thiogalactopyranoside; LB, Luria−Bertani; MOPS, 3-(*N*-morpholino)propanesulfonic acid; NiNTA, nickel nitrilotriacetic acid; PCR, polymerase chain reaction; Tris, tris-(hydroxymethyl)aminomethane; SAH, *S*-adenosylhomocysteine; SAM, *S*-adenosylmethionine; dTDP, thymidine 5′-diphosphate, dTMP, thymidine 5′-monophosphate.

 Published on Web 12/13/2010

Scheme 1

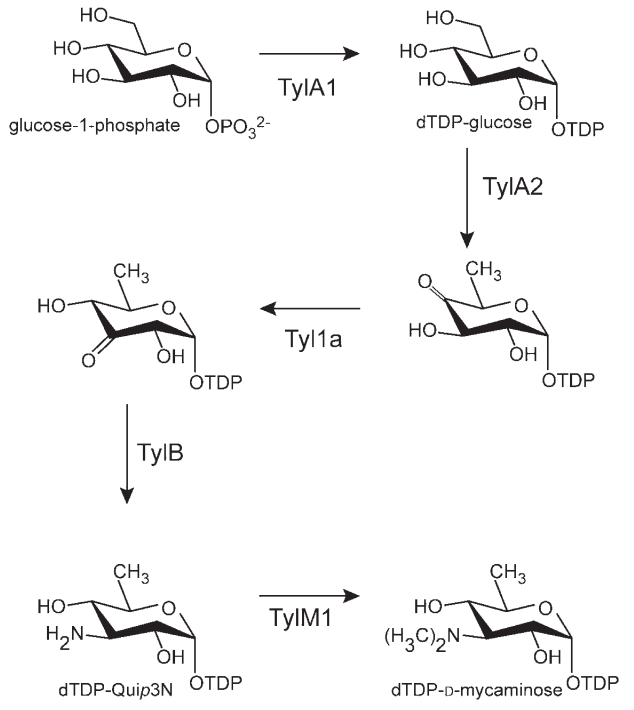

substrate, dTDP-3-amino-3,6-dideoxyglucose or dTDP-Qui*p*3N. In addition to these structural studies, the role of His 123 in catalysis was probed via site-directed mutagenesis and kinetic analyses.

MATERIALS AND METHODS

Enzymatic Synthesis of dTDP-Quip3N. dTDP-Qui*p*3N was synthesized using dTDP-glucose as the starting material. The 4,6-dehydratase (RmlB) from *Escherichia coli*, the 3,4-ketoisomerase (QdtA) from *Thermoanaerobacterium thermosaccharolyticum* E207-71, and the aminotransferase (DesV) from *S. venezuelae* required for the synthesis of dTDP-Qui*p*3N were previously purified in the laboratory. A typical 10 mL reaction mixture contained 20 mM HEPPS (pH 8.5), 100 mM NaCl, 5 mM $MgCl_2$, 100 mg of dTDP-glucose, 250 mg of glutamate, 4 mg of RmlB, 2 mg of QdtA, and 25 mg of DesV. The reaction was allowed to proceed at 37 °C for 5.5 h. All enzymes were removed using a 10 kDa cutoff Millipore Centriprep concentrator, and the enzyme-free reaction products were diluted 1:10 with water. Purification was achieved with an ÄKTA Purifier HPLC (GE Healthcare) equipped with a Resource-Q 6 mL anion-exchange column (GE Healthcare) and using a 120 mL gradient from 1 to 250 mM ammonium bicarbonate at pH 8.5. The desired product peak was identified by ESI mass spectrometry (*m*/*z* 546 amu). Fractions correlating to the product peak were pooled and lyophilized to remove all traces of buffer.

Cloning, Expression, and Purification. *S. fradiae* (ATCC 19609) was obtained from the American Type Culture Collection. Cultures were grown at 26 °C in ISP Medium 1 for 7 days. Genomic DNA was isolated according to standard protocols, and the gene encoding TylM1 (*tylM1*) was PCR-amplified using the forward primer 5′-AAA*CATATG*GCCCATTCATCCGCCACGGCC-3′ and the reverse primer 5′-AAA*CTCGAG*CCGGGTTTCTCCCTTCGCTCCGG-3′. The purified PCR product was A-tailed and ligated into a pGEM-T (Promega) vector for screening and sequencing. The TylM1-pGEM-T construct of the correct sequence was digested with *Nde*I and *Xho*I, and the *tylM1* gene was ligated into a pET31 (Novagen) plasmid, which resulted in the production of a C-terminal hexahistadine-tagged protein.

The TylM1-pET31 plasmid was used to transform modified BL21 *E. coli* cells (Invitrogen). Cultures in LB media were grown at 37 °C until an optical density of ~0.6 at 600 nm was achieved. The cultures were subsequently cooled to 23 °C, and expression of TylM1 was induced by the addition of 1.0 mM IPTG. Protein expression was allowed to proceed for 18 h. TylM1 was purified at 4 °C using Ni-NTA resin from Qiagen following standard procedures. Purified TylM1 was dialyzed against 25 mM Tris and 100 mM NaCl at pH 8.0. Following dialysis, the protein was concentrated to 42.5 mg/mL on the basis of the extinction coefficient 1.487 $(mg/mL)^{-1}$ cm^{-1} at 280 nm. For storage, the protein was flash frozen in liquid nitrogen.

All point mutations of the *tylM1* gene were introduced via the Stratagene QuikChange method, and the plasmids were sequenced to verify that no additional changes had been introduced. The two mutant proteins used in this investigation, H123N and H123A, were prepared and purified in a similar manner as described above.

Structural Analysis of TylM1. Crystallization conditions were initially surveyed via the hanging drop method of vapor diffusion and using a sparse matrix screen developed in the laboratory. For the TylM1/SAM/dTDP-phenol complex, X-ray diffraction quality crystals were obtained by mixing, in a 1:1 ratio, the protein (at 18 mg/mL with 5 mM SAM and 5 mM dTDP-phenol) and a solution containing 22% monomethyl ether poly(ethylene glycol) 5000, 2% 2-propanol, and 100 mM MOPS (pH 7.0). The crystals belonged to the space group *C*2 with unit cell dimensions of a = 88.1 Å, b = 41.4 Å, c = 86.6 Å and β = 121.2°. The asymmetric unit contained one subunit. The stabilization solution required for cryocooling contained 28% monomethyl ether poly(ethylene glycol) 5000, 10% ethylene glycol, 100 mM NaCl, 5 mM SAM, 5 mM dTDP-phenol, and 100 mM MOPS (pH 7.0).

For preparation of the TylM1/dTDP-Qui*p*3N/SAH complex, crystals previously grown in the presence of SAM and dTDP-phenol were transferred to a solution containing 22% monomethyl ether poly(ethylene glycol) 5000, 100 mM NaCl, 5 mM SAM, and 100 mM MOPS (pH 7.0) for 2 days to remove the dTDP-phenol. These crystals were subsequently transferred to a second solution containing 22% monomethyl ether poly(ethylene glycol) 5000, 100 mM NaCl, 5 mM SAM, 10 mM dTDP-Qui*p*3N, and 100 mM MOPS (pH 7.0) and allowed to equilibrate overnight. The crystals belonged to the space group $P2_1$ with unit cell dimensions of a = 86.6 Å, b = 41.1 Å, c = 87.3 Å, β = 117.9°, and one dimer in the asymmetric unit. The stabilization solution required for cryocooling contained 28% monomethyl ether poly(ethylene glycol) 5000, 10% ethylene glycol, 100 mM NaCl, 5 mM SAM, 10 mM dTDP-Qui*p*3N, and 100 mM MOPS (pH 7.0). Note that although SAM was included in the crystallization trials, only SAH was observed bound in the active site.

Crystals of the site-directed mutant proteins were grown in the presence of 5 mM SAM and 10 mM dTDP-Qui*p*3N under similar conditions as those described for the TylM1/dTDP-Qui*p*3N/SAH complex except at pH 7.5 rather than 7.0. They also belonged to the space group $P2_1$ with similar unit cell dimensions.

All high-resolution X-ray data sets were collected at 100 K with a Bruker AXS Platinum 135 CCD detector equipped with Montel optics and controlled by the Proteum software suite (Bruker AXS Inc.). The X-ray source was Cu Kα radiation from

Table 1: X-ray Data Collection Statistics

	wild-type protein complexed with SAM and dTDP-phenol	wild-type protein complexed with SAH and dTDP-Qui*p*3N	H123A mutant protein complexed with SAH and dTDP-Qui*p*3N	H123N mutant protein complexed with SAH and dTDP-Qui*p*3N
resolution limits	36.4−1.35 (1.44−1.35)[a]	44.8−1.79 (1.83−1.79)[a]	43.6−1.80 (1.90−1.80)[a]	77.1−1.65 (1.75−1.65)[a]
no. of independent reflections	55697 (9141)	50868 (7031)	47224 (6250)	60958 (8728)
completeness (%)	94.3 (87.5)	98.5 (93.2)	93.4 (83.3)	93.4 (83.4)
redundancy	3.2 (1.6)	4.2 (2.4)	2.8 (1.5)	3.4 (1.5)
avg I/avg $\sigma(I)$	13.7 (2.6)	10.2 (1.8)	8.7 (2.0)	9.6 (1.8)
R_{sym} (%)[b]	4.7 (21.3)	8.5 (43.6)	7.5 (30.5)	8.1 (39.0)

[a]Statistics for the highest resolution bin. [b]$R_{sym} = (\sum|I - \bar{I}|/\sum I) \times 100$.

Table 2: Least-Squares Refinement Statistics

	wild-type protein complexed with SAM and dTDP-phenol	wild-type protein complexed with SAH and dTDP-Qui*p*3N	H123A mutant protein complexed with SAH and dTDP-Qui*p*3N	H123N mutant protein complexed with SAH and dTDP-Qui*p*3N
resolution limits (Å)	100−1.35	100−1.79	100−1.8	100−1.65
R-factor[a] (overall) (%)/no. of reflections	18.5/55697	21.2/50622	18.6/47216	19.7/60948
R-factor (working) (%)/no. of reflections	18.3/52903	20.9/48053	18.3/44824	19.4/57875
R-factor (free) (%)/no. of reflections	20.9/2794	26.6/2569	24.5/2392	24.5/3073
no. of protein atoms	1842[b]	3679[d]	3660[f]	3688[h]
no. of heteroatoms	334[c]	604[e]	513[g]	544[i]
average B value (Å^2)				
protein atoms	15.3	20.0	16.1	15.6
ligands	9.3	13.0	9.6	8.3
solvent	26.6	31.9	25.9	27.3
weighted rms deviations from ideality				
bond lengths (Å)	0.012	0.012	0.013	0.014
bond angles (deg)	2.2	2.1	2.3	2.3
planar groups (Å)	0.008	0.010	0.014	0.014

[a]R-factor $= (\sum|F_o - F_c|/\sum|F_o|) \times 100$, where F_o is the observed structure factor amplitude and F_c is the calculated structure factor amplitude. [b]These include a multiple conformation for Glu 191. [c]Heteroatoms include a dTDP-phenol molecule, a SAM molecule, an ethylene glycol molecule, and 272 waters. [d]These include a multiple conformation for Arg 183 in subunit 1. [e]Heteroatoms include two dTDP-Qui*p*3N molecules, two SAH molecules, an ethylene glycol molecule, and 478 waters. [f]These include a multiple conformation for Arg 183 in subunit 1. [g]Heteroatoms include two dTDP-Qui*p*3N molecules, two SAH molecules, an ethylene glycol molecule, and 387 waters. [h]These include multiple conformations for Arg 183 in subunit 1 and Arg 90, Asn 123, and Glu 191 in subunit 2. [i]Heteroatoms include two dTDP-Qui*p*3N molecules, two SAH molecules, two ethylene glycol molecules, and 414 waters.

a Rigaku RU200 X-ray generator operated at 50 kV and 90 mA. All data sets were processed with SAINT version 7.06A (Bruker AXS Inc.) and internally scaled with SADABS version 2005/1 (Bruker AXS Inc.). X-ray data collection statistics are presented in Table 1.

The structure of the TylM1/dTDP-phenol/SAM complex was solved via molecular replacement with the program Phaser (*12*) and using as a search probe the X-ray coordinates for DesVI (*9*). A preliminary model was constructed with the software package COOT (*13*). Refinement of the model with REFMAC (*14*) led to a final overall R-factor of 18.5% for all measured X-ray data from 30 to 1.35 Å resolution. The electron densities corresponding to the ligands were unambiguous in the early stages of refinement, and thus they were included in the model at the beginning of the refinement process. The structure of the TylM1/dTDP-Qui*p*3N/SAH complex was determined by molecular replacement using the TylM1/dTDP-phenol/SAM model as a search probe with the ligands removed. The model was refined to an overall R-factor of 21.2% at 1.79 Å resolution. The H123A and H123N mutant protein structures were solved by molecular replacement and refined with REFMAC. Relevant refinement statistics are given in Table 2.

Activity Assays. Steady-state kinetic parameters, as presented in Table 3, were determined using the SAM510:SAM methyltransferase assay kit (G Biosciences). The assay was continuously monitored with a Beckman DU 640B spectrophotometer. The SAM510 assay protocol was followed with the exception that a 100 μL reaction was used in a 1 cm 100 μL cuvette at 25 °C. The kit components included an assay buffer, an enzyme mix, a colorimetric mix, and *S*-adenosylmethionine. These were incubated at 37 °C and subsequently cooled to 25 °C prior to the addition of TylM1 and dTDP-Qui*p*3N. The production of *S*-adenosylhomocysteine was monitored at 510 nm (ε = 26.0 mM^{-1} cm^{-1}) at 25 °C every 5 s over 30 min. Concentrations of TylM1 used were 0.225, 0.75, and 2 μM for the wild type, H123A mutant, and H123N mutant proteins, respectively. dTDP-Qui*p*3N concentrations ranged from 0.007 to 0.5 mM for the wild-type protein, 0.1 to 7 mM for the H123A mutant

Table 3: Steady-State Kinetic Parameters

enzyme	K_m(dTDP-Qui*p*3N) (mM)	k_{cat} (s^{-1})	k_{cat}/K_m (M^{-1} s^{-1})
TylM1	0.045 ± 0.004	0.172 ± 0.004	(3.8 ± 0.3) × 10^3
H123A mutant protein	0.67 ± 0.05	0.046 ± 0.001	69 ± 5
H123N mutant protein	0.93 ± 0.08	0.0126 ± 0.0003	14 ± 1

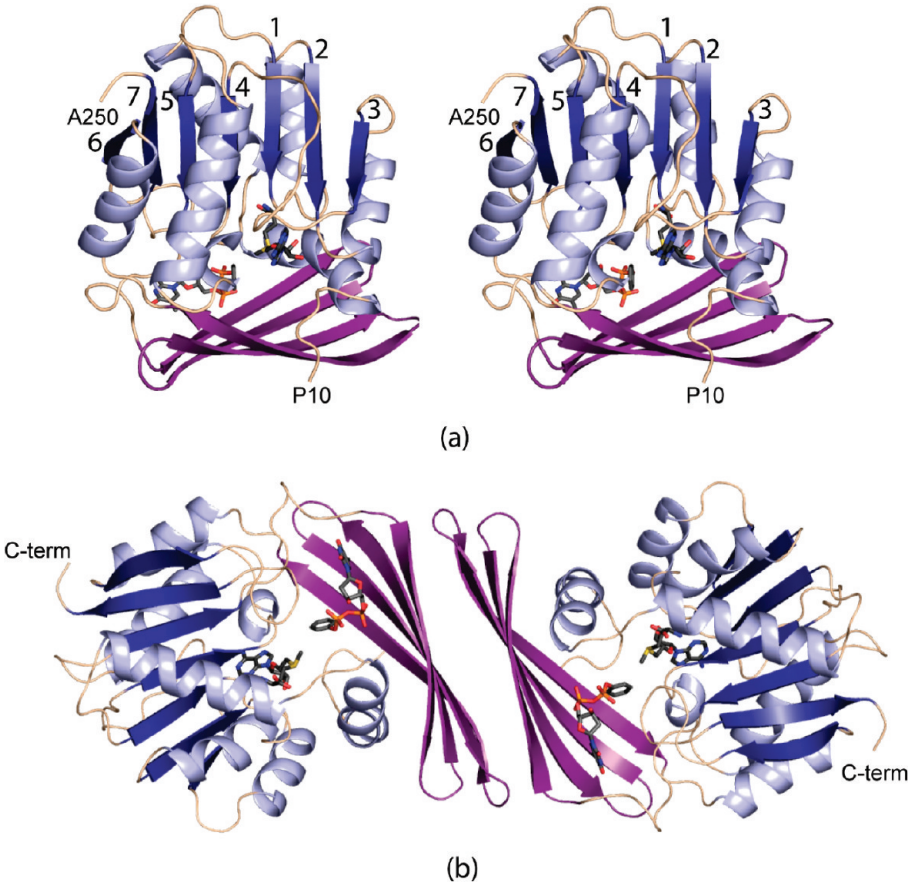

FIGURE 1: The structure of TylM1. A ribbon representation of one subunit of TylM1 is presented in (a). The "SAM-binding" domain is highlighted in light and dark blue, whereas the dimerization domain is shown in violet. SAM and dTDP-phenol are displayed in stick representations. The dimeric structure of TylM1 is shown in (b). All figures were prepared with PyMOL (*17*).

protein, and 0.1 to 10 mM for H123N mutant protein. Kinetic data for each enzyme were fit to eq 1 using Sigma Plot 8.

$$v = VA/(K_a + A) \quad (1)$$

RESULTS AND DISCUSSION

Structure of the TylM1/SAM/dTDP-phenol Complex. Previous biochemical studies have demonstrated that TylM1 functions as a dimer (*11*). For this structural analysis, the enzyme crystallized in the space group *C*2 with its local 2-fold rotational axis coincident to a crystallographic dyad, thereby leading to one subunit in the asymmetric unit. Overall, the electron density was very well ordered from Pro 10 to Ala 250 (the first nine N-terminal and the last five C-terminal residues were not visible in the electron density map). The quality of the model, refined to 1.35 Å resolution and an overall *R*-factor of 18.5%, was excellent with 91.6% and 8.4% of the ϕ,ψ angles lying within the core and allowed regions of the Ramachandran plot, respectively, according to PROCHECK (*15*).

A ribbon representation of the TylM1 subunit is presented in Figure 1a. It has overall dimensions of ~60 Å × 35 Å × 50 Å and adopts a two-domain motif. The N-terminal domain contains a seven-stranded mixed β-sheet flanked on each side by two and three α-helices, respectively. This β-sheet is a modified form of the canonical "SAM-binding" fold due to an insertion following β-strand 5 that leads to the four-stranded antiparallel β-sheet comprising the C-terminal domain. The SAM cofactor abuts the first three β-strands of the N-terminal domain whereas the dTDP-phenol is situated between the last four β-strands of the N-terminal domain and the C-terminal region. Shown in Figure 1b is the complete TylM1 dimer. Approximately 750 Å^2 of the subunit surface area is buried upon dimerization. The dTDP-phenol ligands are separated by ~28 Å.

Electron densities corresponding to the bound ligands are shown in Figure 2a. As can be seen, the conformations of both ligands are well-defined. The methyl group of SAM lies at 3.4 Å from $C^{\epsilon 2}$ of dTDP-phenol. A close-up view of the active site near the SAM binding site is presented in Figure 2b. The adenine ring is surrounded by two water molecules, the side chain of Asp 101, and the backbone amide group of Met 102. The adenine ribose, which adopts the $C_{2'}$-*endo* pucker, lies within hydrogen-bonding distance to a water molecule and the carboxylate of Glu 79. A water molecule and the side chains of Tyr 22 and Tyr 33 hydrogen bond to the carboxylate group of SAM, whereas its amino group is positioned within 3.2 Å of two waters and the backbone carbonyl group of Ala 58. In Figure 2c, a close-up view of the binding pocket for dTDP-phenol is presented. The thymine ring hydrogen bonds to two water molecules and the backbone amide group of Thr 159. It also forms a stacking interaction with the indole side chain of Trp 153. Three well-ordered water molecules surround the C-3 hydroxyl moiety of the thymine ribose. Lys 29, Arg 177, Ser 179, and Arg 241 serve to position the pyrophosphoryl group of dTDP-phenol into the active site. Four water molecules also lie within 3.2 Å of the pyrophosphoryl moiety.

As expected from their amino acid sequence identities, the overall folds of TylM1 and DesVI are similar as highlighted in Figure 3. These two proteins superimpose with a root-mean-square deviation of 0.71 Å for 211 structurally equivalent

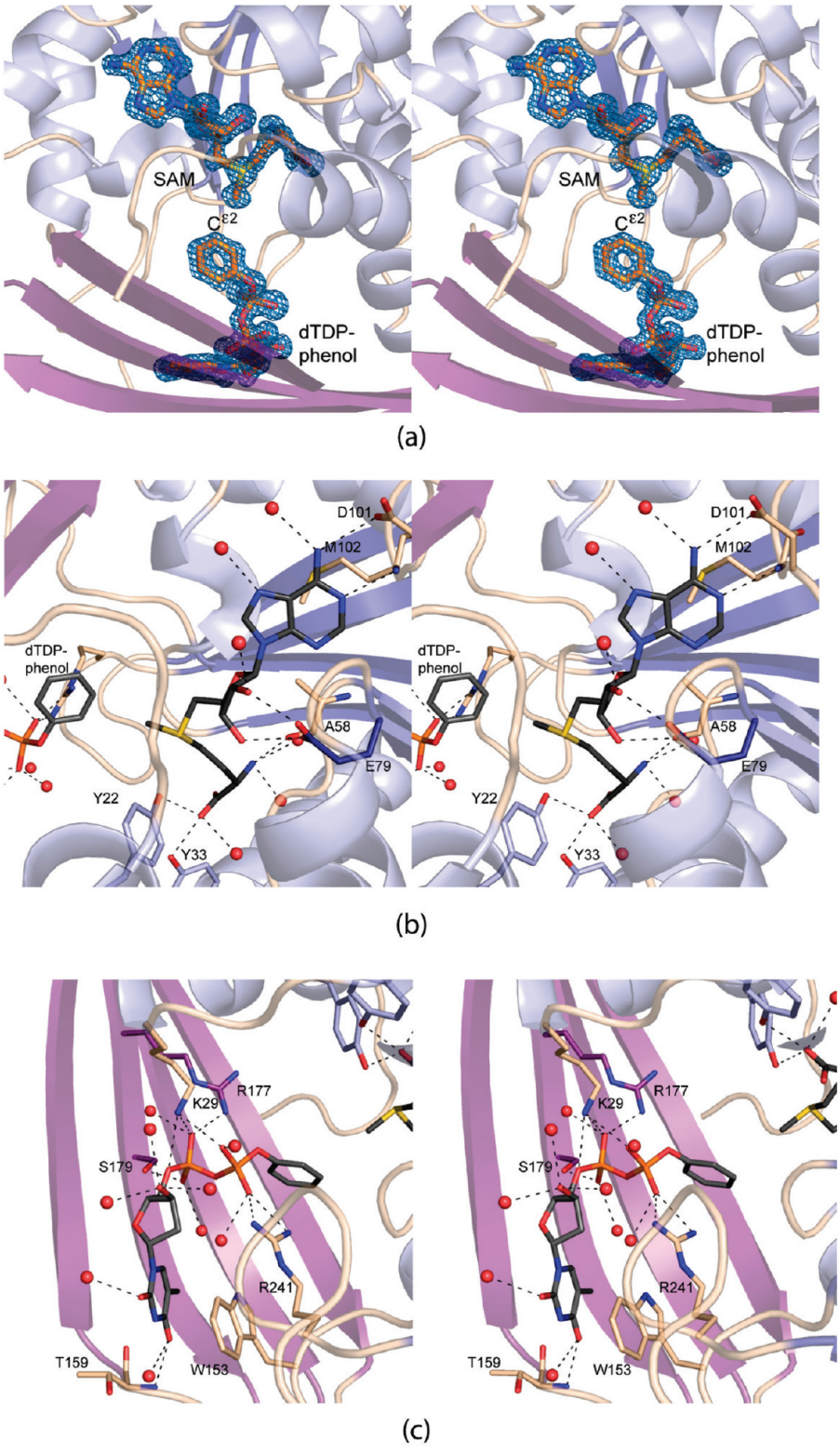

FIGURE 2: Active site of the TylM1/SAM/dTDP-phenol complex. The electron densities corresponding to the SAM and dTDP-phenol ligands are shown in (a). The map was contoured at 2.5σ and calculated with coefficients of the form ($F_o - F_c$), where F_o was the native structure factor amplitude and F_c was the calculated structure factor amplitude. Potential hydrogen-bonding interactions within 3.2 Å between the protein and SAM are depicted as dashed lines in (b). Ordered water molecules are drawn as spheres. A close-up view of the dTDP-phenol binding pocket is displayed in (c). The dashed lines indicate potential hydrogen-bonding interactions.

α-carbons. The only major difference between these two proteins occurs at the N-terminus. In TylM1, the N-terminus curls toward the active site pocket (Figure 3). Whereas this difference does not affect the overall quaternary structures shared by these two enzymes, it does influence their active site pockets as discussed below.

Structure of the TylM1/SAM/dTDP-Quip3N Complex. Crystals of this complex belonged to the space group $P2_1$ with a complete dimer in the asymmetric unit. The structure was solved to 1.79 Å resolution and refined to an overall *R*-factor of 21.2%. Again, the model was excellent with 91.1% and 8.9% of the ϕ,ψ angles for the dimer lying with the core and allowed regions of the

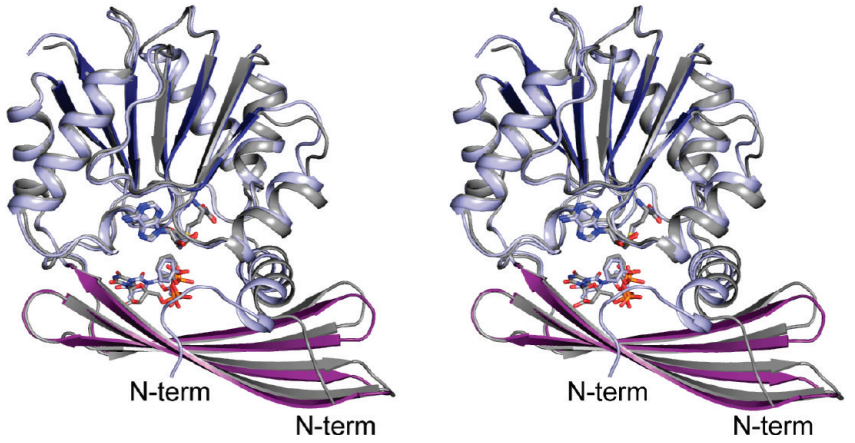

FIGURE 3: Comparison of TylM1 and DesVI. In this superposition, the ribbon representation for DesVI is shown in gray whereas that for TylM1 is depicted in the coloring scheme used in Figure 1. X-ray coordinates for DesVI were determined in this laboratory and deposited in the Protein Data Bank, accession no. 3BXO. Only the positions of the N-termini differ significantly between these two *N*,*N*-dimethyltransferases.

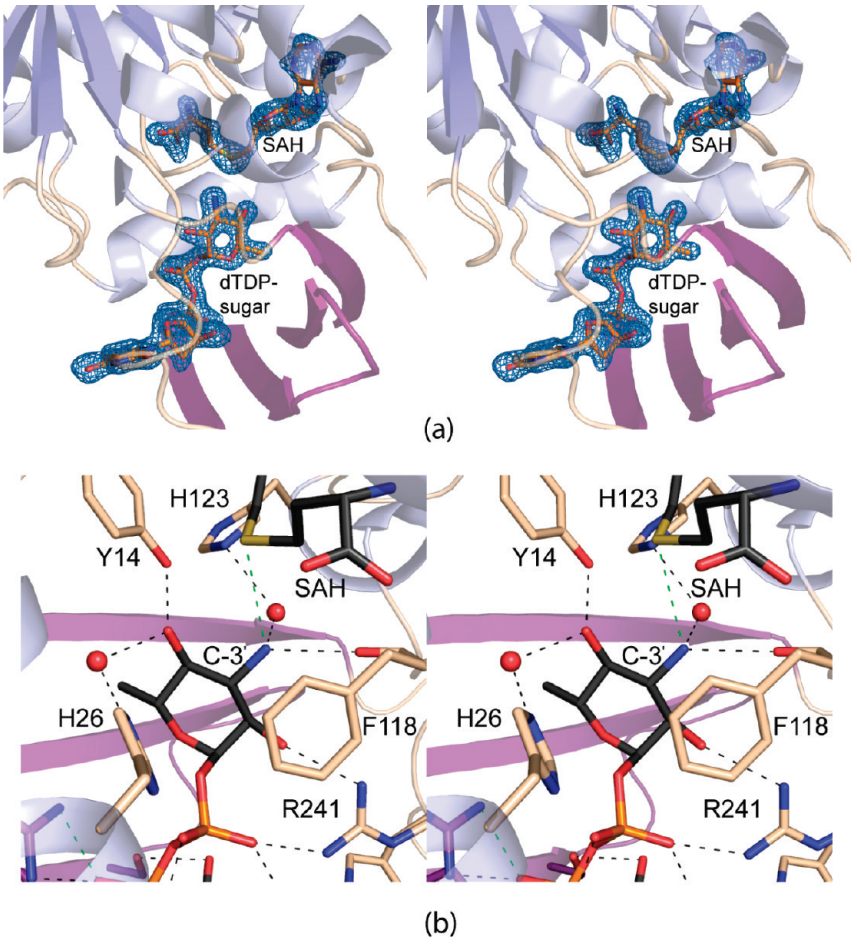

FIGURE 4: Active site of the TylM1/SAH/dTDP-Qui*p*3N complex. The electron densities corresponding to the SAH and dTDP-Qui*p*3N ligands are shown in (a). The map was contoured at 2.5σ and calculated with coefficients of the form ($F_o - F_c$), where F_o was the native structure factor amplitude and F_c was the calculated structure factor amplitude. Potential hydrogen bonds between the protein and the hexose moiety of dTDP-Qui*p*3N are indicated by the dashed lines in (b). Water molecules are represented as red spheres. The green dashed line indicates a distance of 3.6 Å between the amino group of the sugar and the sulfur of SAH.

Ramachandran plot, respectively. The two subunits of the dimer superimpose with a root-mean-square deviation of 0.19 Å for 231 structurally equivalent α-carbons. Given this high structural correspondence, the following discussion refers only to subunit 1 in the X-ray coordinate file.

The electron densities for SAH and the dTDP-linked sugar are displayed in Figure 4a, and as can be seen, the electron density for the dTDP-linked sugar is very well ordered, whereas that for SAH is somewhat weaker, suggesting perhaps a lower occupancy. Within experimental error, however, the manners in which SAM and SAH are accommodated within the TylM1 active site cleft are identical. Shown in Figure 4b is a close-up view of the binding site for the dTDP-linked sugar and, in particular, for the Qui*p*3N moiety. The guanidinium group of Arg 241 hydrogen

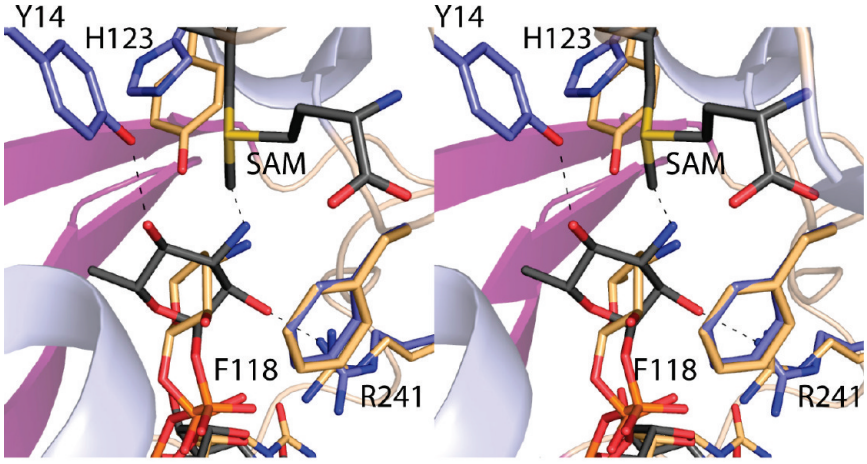

FIGURE 5: Comparison of sugar binding to TylM1 and DesVI. In the initial structural investigation of DesVI, we presented a model for sugar binding based on the observed locations of SAM and UDP-phenol in the active site. This "predicted" model is colored in light orange bonds. The position of the dTDP-Qui*p*3N ligand, when bound to TylM1, is drawn in gray bonds. The TylM1 side chains are shown in blue. The predicted model for DesVI was incorrect by a rotation of approximately 90°. Note that Tyr 14 in TylM1 is not conserved in DesVI, and this is in keeping with the fact that the DesVI substrate does not have a hydroxyl group at the C-4′ position. Arg 241 is conserved, however, and this residue in TylM1 participates in a hydrogen bond with the C-2′ hydroxyl group of the sugar. Most likely, this arginine residue in DesVI also serves in such capacity.

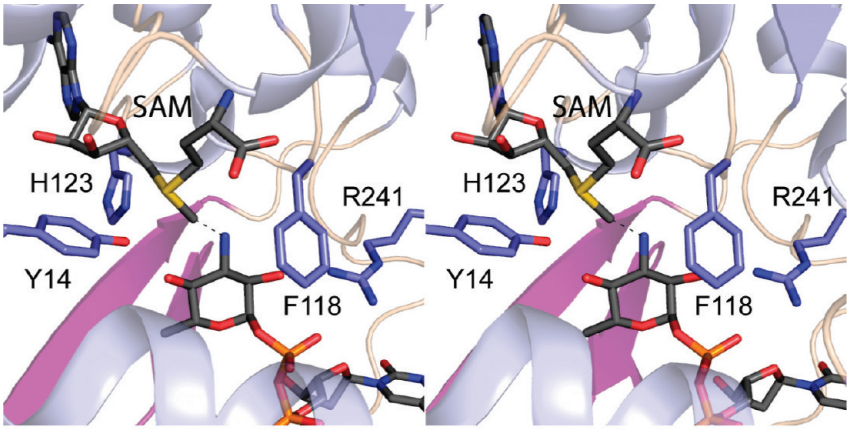

FIGURE 6: Close-up view of the TylM1 active site with SAM and dTDP-Qui*p*3N. For this figure the two ternary complexes described in this report were superimposed to show the relationship between SAM and dTDP-Qui*p*3N.

bonds to the C-2′ hydroxyl group of the hexose, and this residue is conserved in DesVI. In TylM1, the C-4′ hydroxyl group of the hexose is hydrogen bonded by Tyr 14 and a water molecule. Tyr 14 belongs to the N-terminal region that folds into the active site of TylM1 but curls outward in the DesVI structure (Figure 3). The substrate for DesVI lacks a hydroxyl group at the C-4′ position, and most likely TylM1 and DesVI evolved to accommodate these different substrates. The C-3′ amino group of dTDP-Qui*p*3N that is ultimately dimethylated lies within hydrogen-bonding distance of the carbonyl group of Phe 118 and a water molecule. It is also located at 3.6 Å from the sulfur atom of SAH.

In the initial investigation of DesVI, a model for its nucleotide-linked sugar substrate was built into the active site based on the observed binding of UDP-phenol to the enzyme (*9*). A superposition of this hypothetical model for DesVI and the TylM1/SAH/dTDP-Qui*p*3N complex structure reported here is presented in Figure 5, and it emphasizes the perils of modeling building. Our model for the position of the hexose moiety was incorrect by ~90°. We originally predicted that, in DesVI, Tyr 14 would form a hydrogen bond to the C-2′ hydroxyl of the sugar (*9*). Most likely, as observed in TylM1, the conserved arginine rather than Tyr 14 plays a key role in substrate positioning in DesVI.

Site-Directed Mutagenesis Studies. The X-ray analysis of the TylM1/SAM/dTDP-phenol complex provided a structural framework for understanding the manner in which SAM is accommodated in the active site cleft. The TylM1/SAH/dTDP-Qui*p*3N complex revealed how the enzyme binds the dTDP-linked sugar. By combining these two structures, a view of the "Michaelis complex" can be obtained as shown in Figure 6. Catalysis by methyltransferases is known to proceed through an S_N2 displacement reaction (*16*), and the amino nitrogen, which sits at 1.9 Å from the reactive methyl group of SAM, is in the proper position for an in-line attack. One question that arises, however, is what residue, if any, serves as an active site base to remove a proton from the amino nitrogen? The only possible candidate is His 123 that hydrogen bonds to a water molecule which in turn hydrogen bonds to the C-3′ amino group (Figure 4b). This residue is not strictly conserved, however, among bacterial dimethyltransferases. For example, in DesVI it is a tyrosine.

In any event, we tested the possible role of this histidine in catalysis by site-directed mutagenesis experiments. For this analysis, His 123 was converted to an alanine or an asparagine. In both cases, the activities of the enzymes were greatly reduced, but each retained some catalytic function (Table 3). With the H123A mutant protein, the K_m for the dTDP-Qui*p*3N substrate

increased by ~15-fold and the k_{cat} demonstrated an approximate 4-fold reduction. To test that these variations in the kinetic constants were not due to changes in the overall fold of the enzyme, the H123A mutant protein was crystallized and its structure determined to 1.8 Å resolution in the presence of SAH and dTDP-Qui*p*3N. The α-carbons for subunit 1 of the H123A mutant protein superimpose onto the wild-type TylM1 with a root-mean-square deviation of 0.13 Å. There were basically no changes in the polypeptide chain or in the manner in which the SAH and dTDP-Qui*p*3N ligands were bound in the active site of the H123A mutant protein. Water molecules simply filled in the position left behind when the imidazole ring of the histidine was changed to a methyl group. Likewise, the H123N mutant protein retained catalytic activity, albeit reduced. Specifically, the K_m for the dTDP-Qui*p*3N substrate increased by ~21-fold, and the k_{cat} demonstrated an approximate 14-fold reduction. The structure of the H123N mutant protein was determined to 1.65 Å resolution, and as in the H123A protein, several water molecules filled in the hole left behind. The wild-type and H123N mutant proteins superimpose with a root-mean-square deviation of 0.15 Å. Given these structural and functional results, we suggest that catalysis by TylM1 most likely proceeds via approximation, and this may be operative in DesVI as well.

In summary, the results reported herein describe for the first time the manner in which an *N,N*-dimethyltransferase involved in unusual sugar biosynthesis accommodates a nucleotide-linked sugar in its active site. The interactions between the hexose of the dTDP-linked sugar and the protein are quite limited, and there is an apparent lack of a catalytic base lying within hydrogen-bonding distance of the sugar's primary amino group. Clearly, the SAM and dTDP-Quip3N are appropriately aligned for a direct in-line displacement reaction. As the two substrates approach, the proton on the C-3′ amino group is most likely transferred to one of the water molecules lining the active site pocket. Given that the reaction of TylM1 involves a dimethylation, it will be of interest to solve its structure in the presence of a monomethylated substrate. Such a structure, in combination with the results presented here, would provide a molecular scaffold for understanding the manner in which this intriguing enzyme accommodates substrates with altered hydrophobic properties. Experiments designed to address this issue are presently underway.

ACKNOWLEDGMENT

We gratefully acknowledge Drs. W. W. Cleland and James B. Thoden for helpful discussions.

REFERENCES

1. Nedal, A., and Zotchev, S. B. (2004) Biosynthesis of deoxyaminosugars in antibiotic-producing bacteria. *Appl. Microbiol. Biotechnol. 64*, 7–15.
2. Rupprath, C., Schumacher, T., and Elling, L. (2005) Nucleotide deoxysugars: essential tools for the glycosylation engineering of novel bioactive compounds. *Curr. Med. Chem. 12*, 1637–1675.
3. Gandecha, A. R., Large, S. L., and Cundliffe, E. (1997) Analysis of four tylosin biosynthetic genes from the tylLM region of the *Streptomyces fradiae* genome. *Gene 184*, 197–203.
4. Melancon, C. E., III, Yu, W. L., and Liu, H. W. (2005) TDP-mycaminose biosynthetic pathway revised and conversion of desosamine pathway to mycaminose pathway with one gene. *J. Am. Chem. Soc. 127*, 12240–12241.
5. Melancon, C. E., III, Hong, L., White, J. A., Liu, Y. N., and Liu, H. W. (2007) Characterization of TDP-4-keto-6-deoxy-D-glucose-3,4-ketoisomerase from the D-mycaminose biosynthetic pathway of *Streptomyces fradiae*: in vitro activity and substrate specificity studies. *Biochemistry 46*, 577–590.
6. Williams, G. J., and Thorson, J. S. (2009) Natural product glycosyltransferases: properties and applications. *Adv. Enzymol. Relat. Areas Mol. Biol. 76*, 55–119.
7. Allard, S. T., Cleland, W. W., and Holden, H. M. (2004) High resolution X-ray structure of dTDP-glucose 4,6-dehydratase from *Streptomyces venezuelae*. *J. Biol. Chem. 279*, 2211–2220.
8. Loenen, W. A. (2006) S-adenosylmethionine: jack of all trades and master of everything? *Biochem. Soc. Trans. 34*, 330–333.
9. Burgie, E. S., and Holden, H. M. (2008) The three-dimensional structure of DesVI from *Streptomyces venezuelae*: a sugar *N,N*-dimethyltransferase required for dTDP-deososamine biosynthesis. *Biochemistry 47*, 3982–3988.
10. Xue, Y., Zhao, L., Liu, H. W., and Sherman, D. H. (1998) A gene cluster for macrolide antibiotic biosynthesis in *Streptomyces venezuelae*: architecture of metabolic diversity. *Proc. Natl. Acad. Sci. U.S.A. 95*, 12111–12116.
11. Chen, H., Yamase, H., Murakami, K., Chang, C. W., Zhao, L., Zhao, Z., and Liu, H. W. (2002) Expression, purification, and characterization of two *N,N*-dimethyltransferases, tylM1 and desVI, involved in the biosynthesis of mycaminose and desosamine. *Biochemistry 41*, 9165–9183.
12. McCoy, A. J., Grosse-Kunstleve, R. W., Adams, P. D., Winn, M. D., Storoni, L. C., and Read, R. J. (2007) Phaser crystallographic software. *J. Appl. Crystallogr. 40*, 658–674.
13. Emsley, P., and Cowtan, K. (2004) Coot: model-building tools for molecular graphics. *Acta Crystallogr., Sect. D: Biol. Crystallogr. 60*, 2126–2132.
14. Murshudov, G. N., Vagin, A. A., and Dodson, E. J. (1997) Refinement of macromolecular structures by the maximum-likelihood method. *Acta Crystallogr., Sect. D: Biol. Crystallogr. 53*, 240–255.
15. Laskowski, R. A., MacArthur, M. W., Moss, D. S., and Thornton, J. M. (1993) PROCHECK: a program to check the stereochemical quality of protein structures. *J. Appl. Crystallogr. 26*, 283–291.
16. Bugg, T. (1997) An Introduction to Enzyme and Coenzyme Chemistry, Blackwell Science Ltd., Oxford.
17. DeLano, W. L. (2002) The PyMOL molecular graphics system, DeLano Scientific, San Carlos, CA.